Characterization and automated detection of waves structures observed from PFISR and GNSS measurements

SRI

For more information:

Olusegun Jonah*, Pablo Reyes, Leslie Lamarche, Anthony van Eyken

SRI International Menlo Park, Menlo Park, CA, United States

AGU Fall Meeting
Chicago, IL
12 -16 December 2022

Final Paper Number: SA45D-2183

Introduction/Instrumentation

We present automated wave characterization and source detection analysis using the Poker Flat Incoherent Scatter Radar (PFISR) and the Global Navigation Satellite System (GNSS) over the high latitudinal region (65^{o}N $\pm$ 5^o latitudes, 147^{o}W $\pm$ 5^o longitudes).

Figure 1. PFISR and GNSS configurations

We analyzed different potential atmospheric forcings, which include the upper atmospheric drivers (e.g. AP, SZA, Dst, and ap) and lower atmospheric drivers (e.g. different components of mean wind (U_i) and temperature (T_i)) to investigate the source of the observed wave perturbations.

We compare different parameters such as horizontal wavelength, wave propagation directions, and velocity observed in PFISR and GNSS-TEC measurements and examine the different seeding sources that generate observable waves in the datasets. This approach will be applied to other GNSS TEC data from receivers around the world and serves as additional input into our innovative machine learning (ML) algorithms designed to characterize the background density and predict wave-like high/low-frequency perturbations anywhere in the global.

Automated Wave detection

PFISR Measurements: Identification of wave activity from PFISR measurements is done using the Probability of false alarm (PFA) obtained from the Lomb-Scargle method. This approached is explained in detail by Negale et. al. (2018). We have modified the Negale algorithm and upgrade the code from a manually wave analysis to an automated operated wave detector.

GNSS Measurements: We utilize GNSS observational data generated by the combined dual frequencies of L1 and L2 along the signal path between a satellite transmitters and receiver stations to calculate the total electron content (TEC). The wave perturbation is obtained by using a band-pass Butterworth filter with order 4 and cutoff frequencies (period) 0.667mHz - 0.277mHz (25 min – 60 min) – MSTID and 0.27mHz - 0.138mHz (60 min – 120 min) – LSTIDs. Different wave parameters are then automatedly computed from corresponding MSTID/LSTID. Figure 2 shows the procedures. We compute the wavelength (λ) and period (τ) by applying spectral analysis and use basic wave equations such as change in displacement (ΔX) over change in time (ΔT) as well as λ / τ, to compute the horizontal phase velocity.

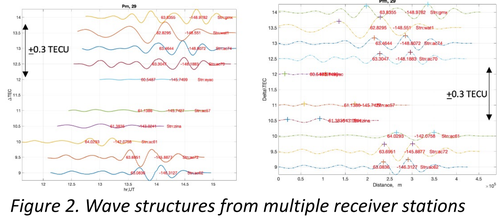

Figure 2. Wave structures from multiple receiver stations viewing PRN 29 is plot as a function of time to obtain the period, represents similar wave structure but plotted as a function of distance to obtain the wavelength.

Wave Parameter Distribution of MSTIDs and LSTIDs

11-year of data (one solar cycle) spanning from 2010 through 2020, extracted from GNSS TEC data using 10 GNSS stations over Poker Flat (65^{o}N $\pm$ 5^o latitudes, 147^{o}W $\pm$ 5^o longitudes) has been used to obtained wave multiple wave parameter distributions (dist). Figure 3 from top to bottom show the period, wavelength, phase velocity, and wave propagation direction Pearson distributions. The blue and red colors represent the MSTIDs and LSTIDs wave dist. respectively.

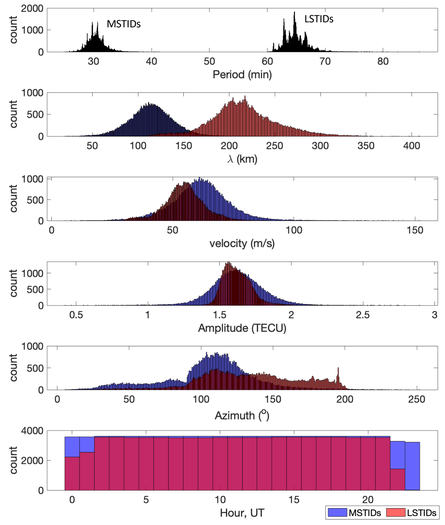

Figure 3. 11 years median dist. of MSTIDs (blue) and LSTIDs (red) wave parameters.

The periodicity shows a normal dist. centered at 25 mins for MSTIDs and 65 mins for LSTIDs. The wavelength also shows two distinct normal dist., while the velocity show an overlapping normal dist. The wave propagation directions however, has a widely spread dist. with mainly south eastward direction.

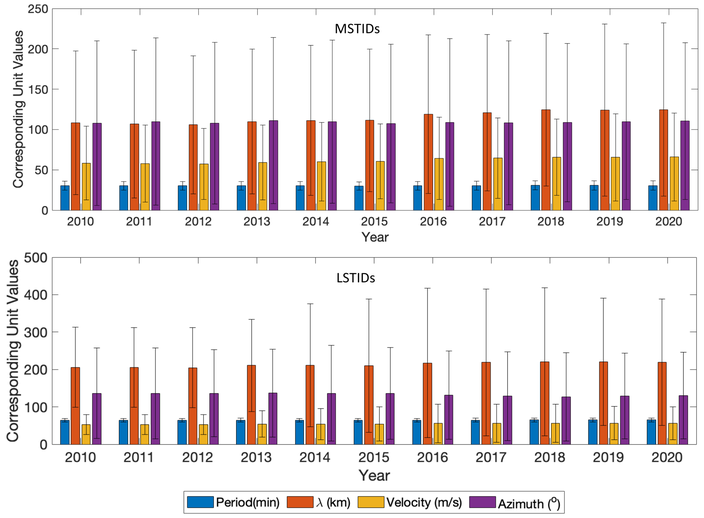

Figure 4. Histogram of yearly median dist. of wave parameters: MSTIDs (top) and LSTIDs (bottom). The error bars represent the minimum and maximum yearly values

MSTIDs and LSTIDs have period between 25 to 55min and 60 to 90min respectively. The max velocity and wavelength for MSTIDs 100ms^{-1}/235 km and LSTIDs 120ms^{-1}/425 respectively, while their propagation direction is predominantly eastward for MSTIDs and south-eastward for LSTIDs.

Comparison of PFISR and GNSS observations: wave parameters

We compared 3-year of wave parameters detected from PFISR measurements with the wave parameters estimated using GNSS-TEC measurements. Work is still in progress to process 11-year of PFISR data in order to carry-out similar quantitative analysis with that of the GNSS-TEC data. Figure 5 from top to bottom show the period, wavelength, phase velocity, and wave propagation direction Pearson distributions.

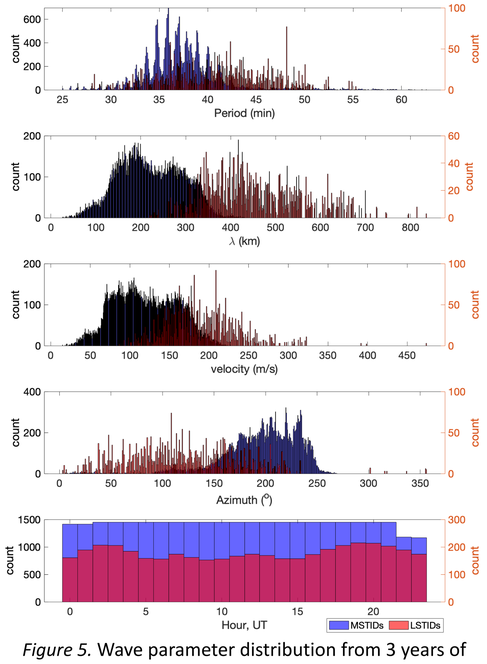

Figure 5. Wave parameter distribution from 3 years of PFISR and GNSS data

The blue and red colors represent the wave parameter distributions from GNSS and PFISR respectively. **Figure 5 shows some agreements in the wave period and velocity in general as illustrated by the largely overlapping distribution. However, there are also some discrepancies in the wavelength and propagation directs as indicated by the widely spread-out of the PFISR data over the GNSS wave parameters.**

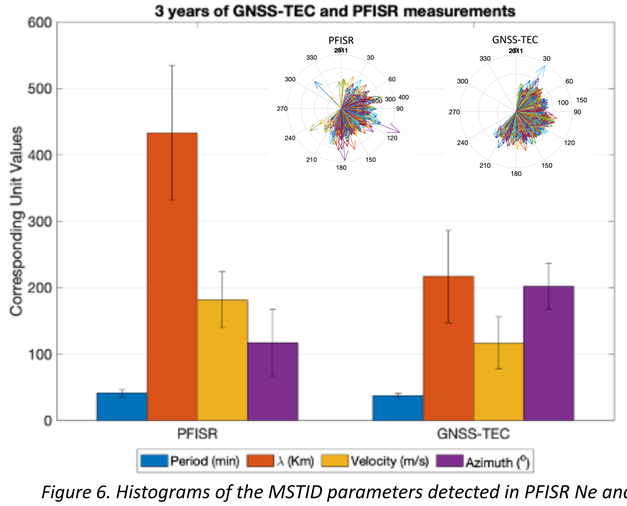

Figure 6. Histograms of the MSTID parameters detected in PFISR Ne and GNSS-TEC measurements – 3-year analysis. The polar plots (top right) show the wave propagation direction for both PFISR and GNSS-TEC

Potential Drivers

We investigated multiple potential drivers obtained from the lower atmosphere (e.g. mean wind, at 2 to 100 hPa) and upper atmosphere (e.g. Dst, ap etc.). This is to help us understand the source of the observed waves perturbation and how they fit into the 11-year distribution. **All the upper atmosphere drivers are filtered by Dst < -30 which indicted the presence of geomagnetic storm. As shown in Figure 7, Oct/2015 shows predominant geomagnetic storm activity. This filter was applied to the LSTID observations and the results are shown below.

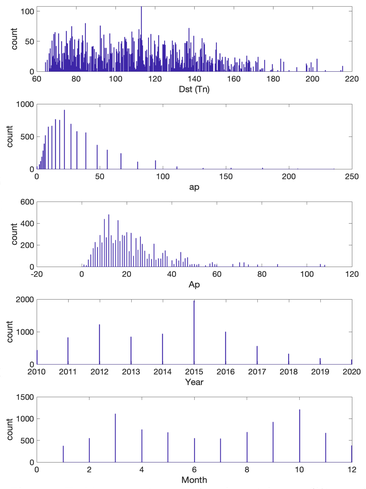

Figure 7. Upper atmospherics drivers filtered with Dst < -30 to identify period with dominant geomagnetic storm activity

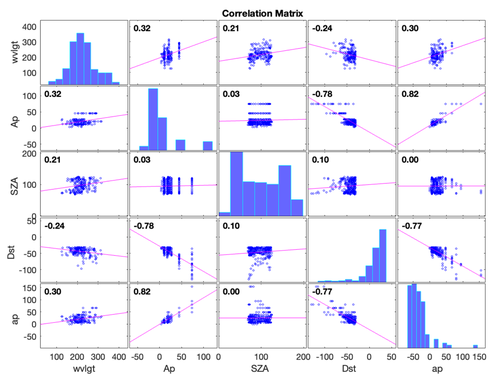

After applying the filter explained above**, **we found some relationship of the LSTIDs wave parameters with the Dst, ap Ap. Similar correlation was not found in the MSTIDs. This is a strong indication/confirmation that LSTIDs are mainly driven by strong geomagnetic storm activities.**

Figure 8. Relationship between LSTID wave parameters and upper atmospheric drivers

Similar analysis were carried out with lower atmospheric drivers. ***All the lower atmospheric drivers are filtered by U_i < 0 which indicted the westward turning of mean wind in the stratosphere and the presence of major SSW.

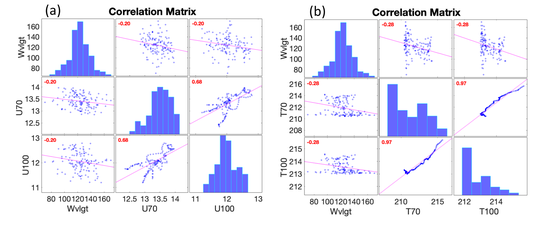

A strong relationship was found in MSTIDs after applying the filter discussed above* but not in the LSTIDs.**

Figure 9. Relationship between LSTID wave parameters and lower atmospheric drivers. (a) and (b) mean wind and Temperature respectively at 70 and 100 hPa.

References/Acknowledgement

Negale, M. R., Taylor, M. J., Nicolls, M. J., Vadas, S. L., Nielsen, K., & Heinselman, C. J. (2018). https://doi.org/10.1029/2017JA024876.

This work is supported by the Advance Research Agency (DARPA) under the contract number: HR001121C0026 and Poker Flat Incoherent Scatter Radar, a major facility funded by the National Science Foundation through cooperative agreement AGS-1840962 to SRI International. PFISR data are available through the SRI International ISR Database at https://amisr.com/database/.